Magnetic Resonance Imaging 74 (2020) 203–212

Contents lists available at ScienceDirect

Magnetic Resonance Imaging

journal homepage: www.elsevier.com/locate/mri

Original Contribution

Cardiac magnetic resonance using fused 3D cine and 4D flow sequences:Validation of ventricular and blood flow measurements

Mehdi H. Moghari[a,b,*], Rob J. van der Geest[c], Maurizio Brighenti[a], Andrew J. Powell[a,b]

[a] Department of Cardiology, Boston Children's Hospital, Boston, MA, USA
[b] Department of Pediatrics, Harvard Medical School, Boston, MA, USA
[c] Department of Radiology, Leiden University Medical Center, Leiden, the Netherlands

ARTICLE INFO

Keywords:
Free-breathing
3D cine
Cardiac MRI
Ventricular function
4D blood flow

ABSTRACT

Purpose: Current cardiovascular magnetic resonance (CMR) examinations require expert planning, multiple breath holds, and 2D imaging. To address this, we sought to develop and validate a comprehensive free-breathing 3D cine function and flow CMR examination using a steady-state free precession (SSFP) sequence to depict anatomy fused with a spatially registered phase contrast (PC) sequence for blood flow analysis.

Methods: In a prospective study, 25 patients underwent a CMR examination which included a 3D cine SSFP sequence and a 3D cine PC (also known as 4D flow) sequence acquired during free-breathing and after the administration of a gadolinium-based contrast agent. Both 3D sequences covered the heart and mediastinum, and used retrospective vectorcardiogram gating (20 phases/beat interpolated to 30 phases/beat) and prospective respiratory motion compensation confining data acquisition to end-expiration. Cardiovascular measurements derived from the 3D cine SSFP and PC images were then compared with those from standard 2D imaging.

Results: All 3D cine SSFP and PC acquisitions were completed successfully. The mean time for the 3D cine sequences including prescription was shorter than that for the corresponding 2D sequences (21 min vs. 36 min, P-value < 0.001). Left and right ventricular end-diastolic volumes and stroke volumes by 3D cine SSFP were slightly smaller than those from 2D cine SSFP (all biases $\leq 5\%$). The blood flow measurements from the 3D and 2D sequences had close agreement in the ascending aorta (bias -2.6%) but main pulmonary artery flow was lower with the 3D cine sequence (bias -11.2%).

Conclusion: Compared to the conventional 2D cine approach, a comprehensive 3D cine function and flow examination was faster and yielded slightly lower left and right end-diastolic volumes, stroke volumes, and main pulmonary artery blood flow. This free-breathing 3D cine approach allows flexible post-examination data analysis and has the potential to make examinations more comfortable for patients and easier to perform for the operator.

1. Introduction

Conventional cardiovascular magnetic resonance (CMR) examinations typically include multiple two-dimensional (2D) cine steady-state free precession (SSFP) acquisitions to assess cardiac chamber volume and function, and multiple 2D phase contrast (PC) acquisitions for the quantification of blood flow [1]. Additional 2D cine SSFP acquisitions may also be performed to assess the thoracic vasculature. Respiratory motion blurring is minimized by having patients repeatedly hold their breath while 1–3 slices are acquired. This conventional CMR approach has several widely-recognized drawbacks. First, its performance requires a knowledgeable operator to prescribe the multiple 2D cardiac imaging planes. This need for specialized cardiac training hinders the adoption of CMR. Second, patient breath-holding is often preferred during the image acquisition to avoid respiratory motion artifacts and blurred images. Breath-holding, however, may not be feasible in ill patients and young children [2]. Even patients who can hold their breath may have difficulty achieving a consistent amplitude leading to

Abbreviations: 2D, 2-dimensional; AAo, Ascending aorta; CMR, Cardiovascular magnetic resonance; DAo, Descending aorta; EDV, End-diastolic volume; EF, Ejection fraction; EPI, Echo planar imaging EPI; ESV, End-systolic volume; GRE, Gradient recalled echo; LPA, Left pulmonary artery; LV, Left ventricle; MPA, Main pulmonary artery; PC, Phase contrast; RPA, Right pulmonary artery; RV, Right ventricle; SENSE, Sensitivity encoding; SV, Stroke volume; SVC, Superior vena cava; SSFP, Steady-state free precession; VENC, Velocity encoding

* Corresponding author at: Department of Cardiology, Boston Children's Hospital, 300 Longwood Avenue, Boston, MA 02115, USA.
E-mail address: mehdi.hedjazimoghari@cardio.chboston.org (M.H. Moghari).

https://doi.org/10.1016/j.mri.2020.09.026
Received 16 March 2020; Received in revised form 31 August 2020; Accepted 27 September 2020
Available online 07 October 2020
0730-725X/

slice-to-slice misregistration and errors in the ventricular volumetric measurements [3]. Newer acceleration techniques mitigate this effect by allowing more slices to be acquired per breath-hold. Third, the need to precisely plan imaging planes and have the patients repeatedly hold their breath prolongs the examination time.

An examination comprised of isotropic resolution 3D cine images acquired during free-breathing addresses these drawbacks as it does not require breath-holding, is easy to plan and, once acquired, can be reformatted into any plane for visualization and quantification of cardiac chambers, blood flow, and the vasculature. Previous approaches to free-breathing 3D cine SSFP [4–9] have a lower temporal resolution than the standard retrospectively-gated 2D cine sequences thereby reducing the fidelity of ventricular volume measurements [10,11]. Furthermore, most use non-linear k-space trajectories, such as radial or spiral, along with parallel imaging acceleration thereby precluding in-line reconstruction by standard scanner equipment. Free-breathing 3D cine PC acquisitions (also known as 4D flow) with respiratory motion compensation have been developed that include data over the entire cardiac cycle [12]. However, anatomic information from these sequences is limited by a low signal-to-noise ratio and low myocardium-to-blood contrast on the magnitude images. This drawback has been overcome by administering an iron-based blood-pool contrast agent, ferumoxytol, resulting in 3D cine PC data that can be used for the assessment of both ventricular function and blood flow [13–16]. Ferumoxytol, however, has been associated with the anaphylactic reactions [17–19] and this has led to restrictions on use and availability in some countries.

In this study, we report an alternative approach to achieving a 3D cine function and flow CMR examination with respiratory motion compensation, coverage of the entire cardiac cycle, and a Cartesian k-space trajectory. Following the administration of a gadolinium-based contrast agent, a 3D cine SSFP sequence using the *Heart-NAV* respiratory gating technique [20,21] is acquired. The contrast agent serves to boost the blood-to-myocardium contrast-to-noise ratio. Then, a 3D cine PC (i.e., 4D flow) sequence also using *Heart-NAV* is acquired with the same anatomic coverage and spatiotemporal resolution as the 3D cine SSFP sequence. Off-line, the 3D SSFP and PC image datasets are spatially registered and the magnitude images of the PC image dataset are discarded. The result is a single 3D cine dataset of high-quality anatomic SSFP images with spatially registered 3D velocity PC data. In this prospective study in patients, we compared cardiovascular measurements derived from this novel 3D cine function and flow CMR examination protocol to those from the standard 2D CMR approach.

2. Methods

2.1. 3D cine heart-NAV technique

A diagram of the *Heart-NAV* technique used for respiratory motion compensation with both the 3D cine SSFP and 3D cine PC spoiled gradient recalled echo (GRE) sequences is shown in Fig. 1. Both sequences are prescribed in a non-angulated sagittal orientation to encompass the heart and mediastinum to at least the lung hili with frequency encoding in the superior-inferior direction. Cardiac motion is resolved by using retrospective vectorcardiogram-gating and k-space binning (segmentation) so that 20 cardiac phases per beat are acquired. Prospective respiratory motion compensation is accomplished using *Heart-NAV* approach [20,21]. Specifically, at the 10th phase (segment) of each cardiac cycle, one excitation radiofrequency pulse is added to read the centerline of k-space along the superior-inferior direction by turning off the phase-encoding gradients and this yields the *Heart-NAV* signal. This signal is collected and transformed from the Fourier domain to the image domain and represents the 1-dimensional projection of the imaging volume along the superior-inferior direction. The *Heart-NAV* image data is processed and displayed using the scanner's standard diaphragm navigator analysis pathway to track respiratory motion. This includes a cross-correlation analysis with the preceding *Heart-NAV* lines to measure displacement in the superior-inferior direction.

As with the conventional diaphragm navigator, the first few seconds at the beginning of the scan are used as a preparation stage to monitor the *Heart-NAV* signal, identify the position of end-expiration and set this position as the reference for the subsequent imaging stage. An acceptance window at end-expiration is then established using this position and an initial width that is pre-specified by the user. Once the *Heart-NAV* preparation stage is complete, the imaging stage begins. If the respiratory position from the *Heart-NAV* signal in a cardiac cycle is within the acceptance window, the acquired 3D cine data for that entire cycle is accepted for reconstruction; otherwise, it is rejected and re-acquired in the next cycle. Also, the width of the acceptance window is adapted during the scan to ensure that scan efficiency does not drop below a pre-specified threshold. A histogram of the respiratory positions from the *Heart-NAV* signal is generated and the width of the acceptance window is either widened or narrowed to ensure that the pre-specified efficiency is maintained [22].

2.2. Spatial registration of 3D cine SSFP and 3D Cine PC images

To create a single 3D cine image dataset with both anatomic and flow data, the 3D cine SSFP images are spatially registered to the magnitude images of the 3D cine PC GRE images. Using MASS research software (V2018-EXP, Leiden University Medical Center), a volume of interest is defined around the heart by manually drawing a contour in a few slices of the 3D cine SSFP images in the first phase of the cardiac cycle (Fig. 2). Using linear interpolation of the defined contours, a volume around the heart is obtained and used as a mask region for the registration algorithm. The 3D cine SSFP images from all 30 timeframes are then registered in 3D space to the magnitude images of the PC GRE dataset using a rigid-body registration algorithm (Elastix registration toolbox) [23]. The 3D cine PC GRE volume is used as the “fixed” image and the 3D cine SSFP volume as the “moving” image. An iterative procedure is executed in which the position and orientation of the 3D cine SSFP volume is adjusted to maximize an image similarity metric, normalized mutual information, within the mask region. The 3D PC GRE velocity data are not altered. Finally, a fused 3D cine dataset is created consisting of the spatially registered 3D cine SSFP images and the x, y, and z-velocity component PC GRE images.

To assess the quality of registration, regions of interest were drawn around the cross-sections of the ascending aorta (primarily an axial image) and the transverse aortic arch (primarily a coronal image) on the magnitude images of 3D cine PC GRE and on the 3D cine SSFP images before and after performing the registration. These 2 locations were chosen so that the analysis would be sensitive to displacement in the superior-inferior, right-left, and anterior-posterior directions. The overlap between the regions of interest on cine PC GRE and cine SSFP images before versus after registration was compared by calculating the Dice coefficient. If the registration is successful, the region of interest overlap should increase and this should be reflected as an increase in the Dice coefficient. To assess whether the registration process altered the flow data, net ascending aorta blood flow measured using only the 3D cine PC GRE dataset was compared to that measured from the fused (registered) image dataset.

2.3. Subjects

To evaluate our free-breathing 3D CMR function and flow technique in clinical practice and compare it to a conventional 2D cine acquisition protocol, we performed a prospective study in patients at Boston Children's Hospital. Patients were eligible if they were referred for a CMR examination with the administration of a gadolinium-based contrast agent. The Boston Children's Hospital Committee on Clinical Investigation approved this study and written informed consent was obtained from all subjects.

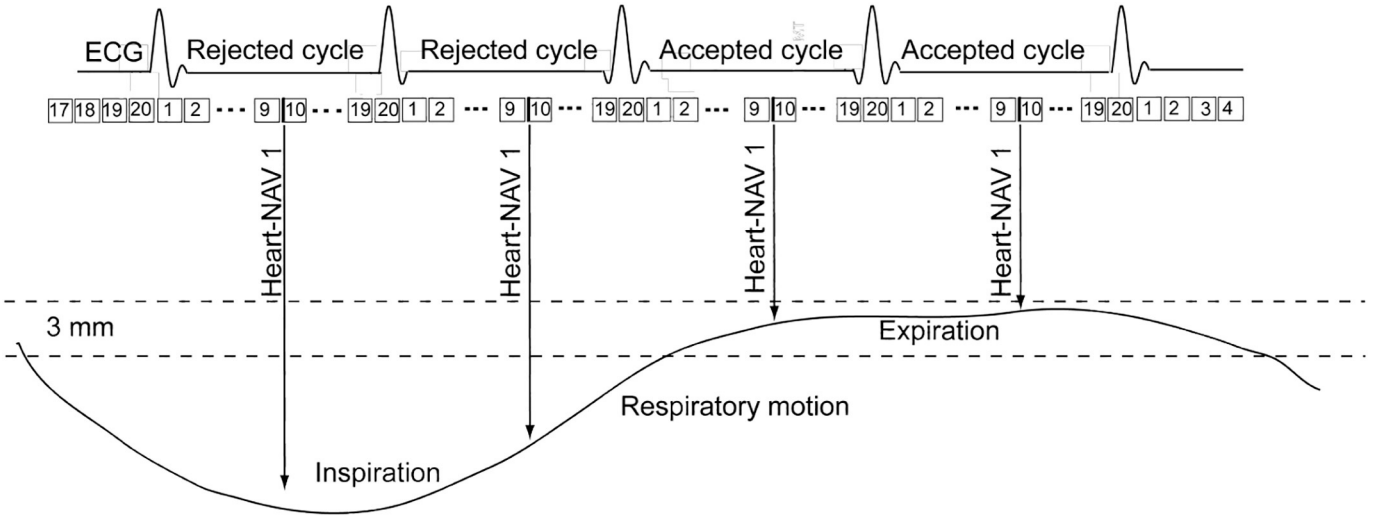

Fig. 1. Diagram of the comprehensive 3D cine function and flow CMR exam which contains steady-state free precession (SSFP) and phase contrast gradient echo (PC GRE) sequences. This exam is performed during free-breathing and Heart-NAV, a respiratory motion compensation technique, is used to prospectively confine the data acquisition to the respiratory end-expiration where only 40% of data within a narrow acceptance window around end-expiration (i.e., 3 mm) is used for image reconstruction.

2.4. CMR protocol

CMR examinations were performed with a 1.5 T Achieva dStream scanner (Philips Healthcare, Best, the Netherlands) and vectorcardiogram gating. In each subject, a standard examination, including 2D cine SSFP and 2D cine PC spoiled GRE (i.e., flow) sequences, was performed. A 2D cine SSFP sequence was used to acquire a stack of ≈12 slices prescribed in a ventricular short-axis plane to completely encompass the left and right ventricles. Imaging was performed with breath-holding at end-expiration for 10–12 s to acquire 2 slices. The acquisition parameters were as follows: field-of-view 260 × 260 mm, in-plane resolution 1.8 × 1.8 mm reconstructed to 1.25 × 1.25 mm, slice thickness 8 mm, slice gap 0–2 mm, flip angle 60°, echo time 1.4 ms, repetition time 2.8 ms, bandwidth 1.1 kHz, heart phases 20 interpolated to 30 and SENSE factor 1–2. A 2D cine flow sequence was used to measure blood flow in the ascending aorta (AAo) and the main pulmonary artery (MPA) during free-breathing with the following imaging parameters: field-of-view 260 × 260 mm, in-plane resolution 1.6 × 1.6 mm reconstructed to 1.1 × 1.1 mm, slice thickness 6 mm, flip angle 12°, echo time 3.3 ms, repetition time 5.2 ms, bandwidth 717.4 Hz, 2 signal averages, velocity encoding (VENC) 100–300 cm/s, heart phases 20 interpolated to 30 and SENSE factor 2.

Three to 15 min after the administration of 0.1–0.15 mmol/kg gadobutrol contrast, a free-breathing 3D cine SSFP sequence with *Heart-NAV* for respiratory motion compensation was acquired in a sagittal plane with the following parameters: field-of-view 512 × 200 × 120 mm, acquired resolution 2.0 × 2.0 × 2.4 mm reconstructed to 1.2 × 1.2 × 1.2 mm, flip angle 60°, echo time 1.5 ms, repetition time 3.0 ms, bandwidth 1.7 kHz, heart phases 20 interpolated to 30, *Heart-NAV* with an adaptive respiratory acceptance window 3 mm, 40% gating efficiency and SENSE factor 3 (2 anterior-posterior direction and 1.5 right-to-left direction). At the end of the examination, a free-breathing 3D cine PC spoiled GRE (i.e., 4D flow) sequence with echo planar imaging (EPI) and *Heart-NAV* for respiratory motion compensation was acquired in a sagittal plane. Its imaging parameters were as follows: field-of-view 512 × 200 × 120 mm, acquired resolution 2.0 × 2.0 × 2.4 mm reconstructed to 1.2 × 1.2 × 1.2 mm, flip angle 10°, echo time 3.3 ms, repetition time 7.4 ms, EPI factor 5, bandwidth 209.7 Hz, heart phases 20 interpolated to 30, *Heart-NAV* with an adaptive respiratory acceptance window 3 mm, 40% gating efficiency, SENSE factor 4 (2 anterior-posterior direction and 2 right-to-left direction) and partial-Fourier (90% along the anterior-posterior and right-to-left directions). The 3D cine PC VENC was chosen to match the highest VENC that was used in the 2D flow

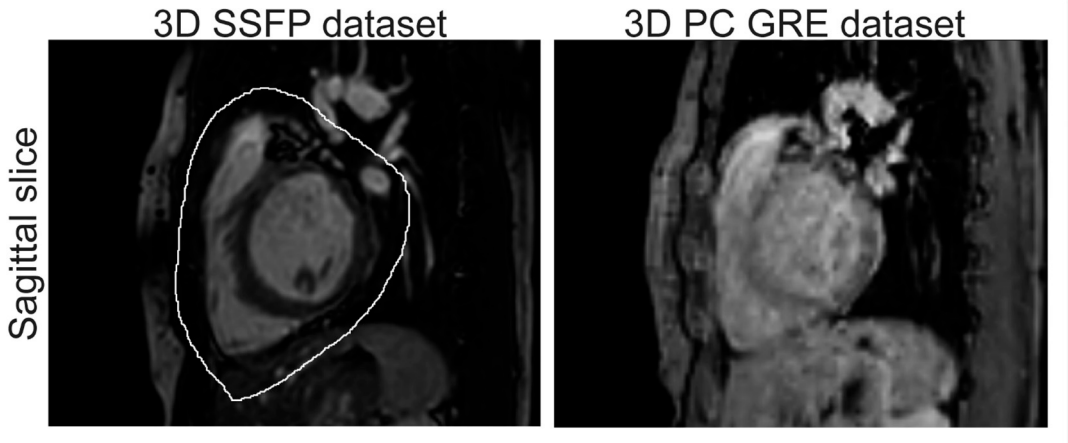

Fig. 2. Magnitude images of 3D cine SSFP and 3D PC GRE (flow) datasets which are used for registration. After the registration is performed, the images of 3D cine SSFP dataset with their better contrast-to-noise ratio between the blood and myocardium replace the magnitude images of the 3D cine PC GRE dataset.

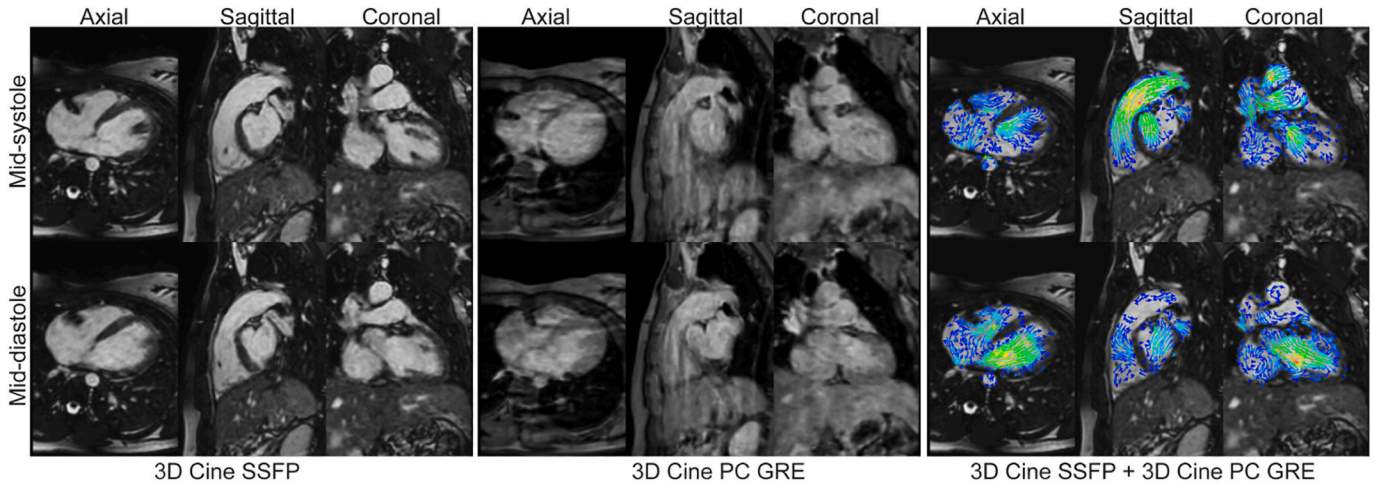

Fig. 3. 3D cine SSFP images, 3D PC GRE images, and their fused registration in a 17-year old patient with a family history of arrhythmogenic ventricular cardiomyopathy.

Table 1
Registration parameters for fusing the 3D cine SSFP and 3D PC GRE datasets (n = 25).

	Rotation (degree)			Translation (mm)		
	RL	AP	SI	RL	AP	SI
Mean	−0.4 ± 0.7	−0.3 ± 0.7	0.3 ± 0.6	0.5 ± 1.0	0.4 ± 1.1	−1.2 ± 1.7
Minimum	−1.7	−2.3	−0.6	−0.8	−1.5	−4.4
Maximum	1.2	0.6	1.7	4.1	3.5	2.4

Values are mean ± standard deviation. AP, anterior-posterior; RL, right-left; and SI, superior-inferior direction.

sequences to avoid aliasing and ranged from 200 to 300 cm/s. For both 3D acquisitions, in-line coil compression was used so that the amount of data was small enough for the scanner to complete the acquisition [24].

The start time for each 2D sequence was recorded from the DICOM header file. By calculating the difference between the start time of two consecutive sequences, the scan time of the first sequence plus any additional preparation time of the next imaging sequence was included. For the 3D cine PC GRE sequence, we could not use the DICOM start time to measure the scan time and preparation time since this sequence was the last performed sequence in the examination. Therefore, for the 3D cine PC GRE sequence and the 3D cine SSFP sequences, we used a stopwatch to prospectively measure scan time. The planning time for both of these sequences is short since the imaging plane is not angulated (straight sagittal).

2.5. Data analysis

All the 3D cine images were reconstructed in-line on the scanner and then transferred to a workstation where the MASS software application was used for spatial registration, reformatting into appropriate views and analysis.

For ventricular volume measurements, a short-axis image stack was generated with a slice thickness of 5 mm (no gap). The right and left ventricular myocardial boundaries on the short-axis reformatted 3D cine images as well as the 2D cine images were delineated by a single observer who was blinded to the numeric results. Left ventricular (LV) and right ventricular (RV) end-diastolic volume (EDV), end-systolic volume (ESV), stroke volume (SV) and ejection fraction (EF) were calculated using a standard summation of disks approach.

For 3D cine-based flow measurements, concomitant gradient correction and phase-offset correction were applied during image reconstruction by the scanner software. Blood flow aliasing artifacts were corrected, when present, using the MASS software. The 2D flow measurements performed were determined by the clinical need and not prespecified. Most of the subjects had 2D blood flow measurements performed in the AAo and MPA. For comparison, the fused 3D cine images were reformatted to an orientation and location that matched the 2D cine flow acquisitions. Contours around the blood vessel were drawn using the magnitude images (originally from the SSFP sequence) and simultaneously displayed on corresponding through-plane velocity-encoded phase images analogous to what is done for 2D cine PC images. For checking the internal measurement consistency within 3D PC data, flow was also measured at the left pulmonary artery (LPA), right pulmonary artery (RPA), superior vena cava (SVC) and descending aorta (DAo). Ventricular stroke volumes were not systematically compared to their respective semilunar valve flow because several patients had atrioventricular valve regurgitation and/or ventricular septal defects.

The 2D versus 3D measurements of the following parameters were compared: LV and RV EDV, ESV, SV, and EF; AAo and MPA net blood flow and pulmonary-to-systemic blood flow ratio (Q_p/Q_s). The internal measurement consistency within the flow data was assessed by comparing MPA flow to the sum of RPA and LPA flow and by comparing AAo flow to the sum of SVC and DAo flow.

2.6. Statistical analysis

Descriptive statistics are reported as median and range, or mean ± standard deviation. A paired two-tailed Student's t-test was used to compare the 2D and 3D cine measurements and a P-value ≤ 0.05 was considered statistically significant. The Pearson correlation coefficient and Bland-Altman analysis were used to assess the extent of correlation and agreement [25]. The mean of the differences (3D-2D) and mean of the differences expressed as a percentage ($\frac{3D-2D}{0.5\times(3D+2D)}\times 100$) were calculated. The amount of internal measurement consistency within the flow datasets was measured using Cronbach's alpha [26].

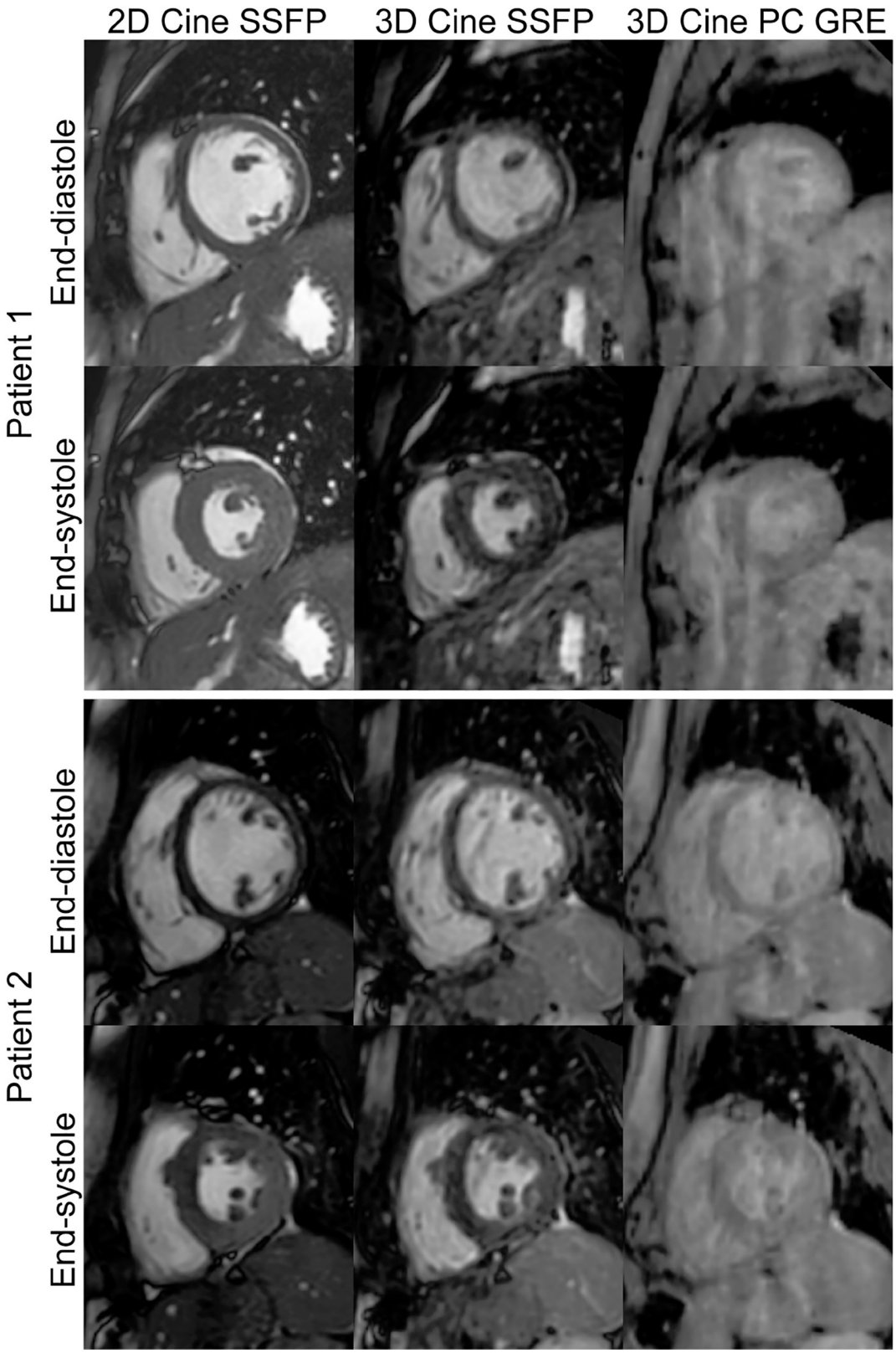

Fig. 4. Mid-ventricular short-axis images in the end-diastole and end-systole acquired using breath-hold 2D cine SSFP images, free-breathing 3D cine SSFP images, and magnitude images of free-breathing 3D cine PC GRE datasets from a 17-year-old female with arrhythmogenic ventricular cardiomyopathy and a 16-year-old female patient with Marfan syndrome.

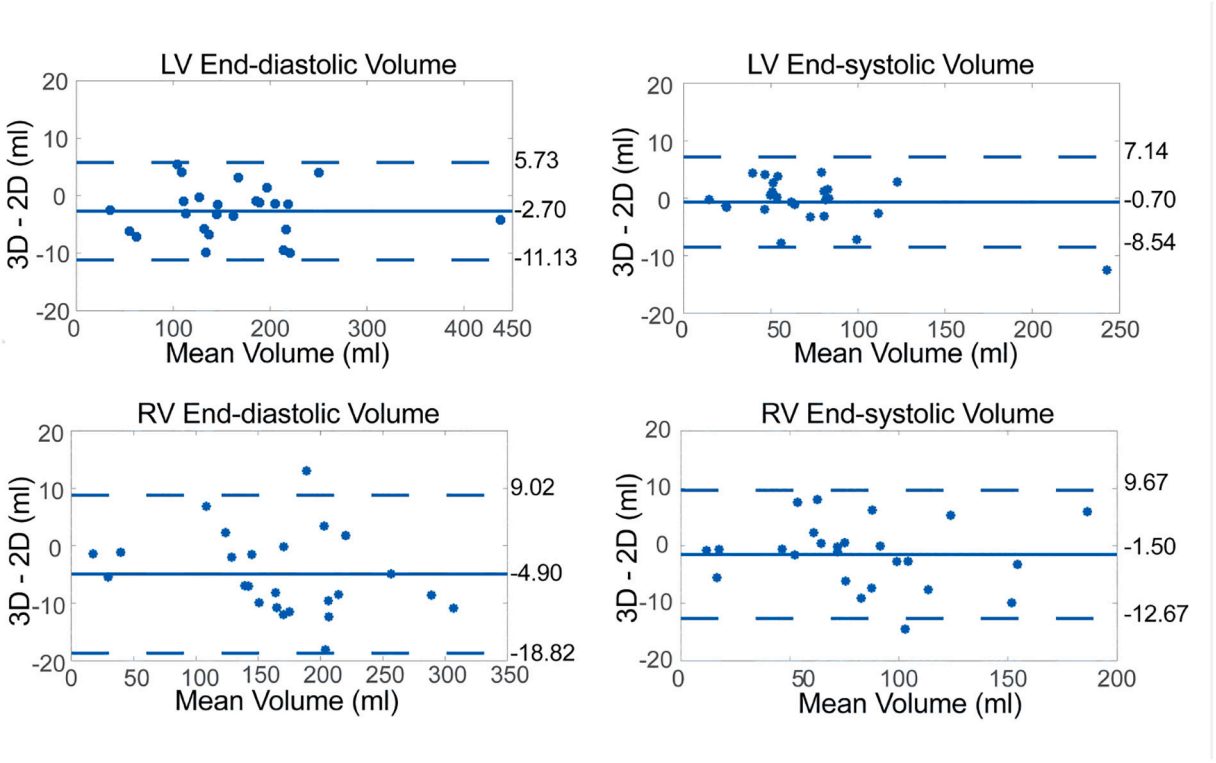

Fig. 5. Bland-Altman plots of agreement comparing left and right ventricular (LV, RV) measurements for the 2D cine SSFP and 3D cine SSFP datasets. The solid line indicates the mean difference (bias) and the dashed lines show ± 1.96 standard deviations of difference.

Table 2
Ventricular measurements for the 2D cine SSFP and 3D cine SSFP sequences (n = 25).

	Left ventricle				Right ventricle			
	EDV (ml)	ESV (ml)	SV (ml)	EF (%)	EDV (ml)	ESV (ml)	SV (ml)	EF (%)
2D cine SSFP	164.1 ± 80.0	71.3 ± 45.4	92.8 ± 38.0	57.8 ± 5.6	169.0 ± 71.8	83.4 ± 42.6	85.6 ± 34.1	50.7 ± 8.3
3D cine SSFP	161.4 ± 79.2	70.6 ± 43.2	90.7 ± 39.8	57.1 ± 5.4	164.0 ± 69.9	81.9 ± 42.1	81.8 ± 32.9	50.3 ± 8.2
Mean difference (3D-2D)	−2.7 ± 4.3	−0.7 ± 4.0	−2.1 ± 4.8	−0.8 ± 2.0	−4.9 ± 7.1	−1.5 ± 5.7	−3.8 ± 5.6	−0.5 ± 2.8
Mean % difference (3D-2D)	−2.3 ± 4.1	−0.4 ± 5.5	−3.7 ± 5.9	−1.3 ± 3.5	−3.5 ± 5.1	−2.6 ± 9.2	−4.6 ± 5.9	−0.9 ± 6.0
Correlation coefficient	0.998	0.997	0.993	0.937	0.995	0.991	0.987	0.940
P-value	0.005	0.410	0.042	0.058	0.002	0.203	0.002	0.425

Values are mean ± standard deviation. EDV, end-diastolic volume; EF, ejection fraction; ESV, end-systolic volume; and SV, stroke volume.

3. Results

3.1. Subjects

Twenty-five patients (9 males) were enrolled in the study and all completed the imaging protocol. Their median age was 24 years (range 2–43 years), the median weight was 62 kg (range 11–129 kg) and the median heart rate during the CMR examination was 76 bpm (range 56–118 bpm). The principal diagnosis for each patient was as follows: aortic coarctation (n = 6), congenital aortic valve disease (n = 4), palliated single ventricle congenital heart disease (n = 3), tetralogy of Fallot (n = 3), truncus arteriosus (n = 2), Ebstein anomaly of the tricuspid valve (n = 1), hypertrophic cardiomyopathy (n = 1), lipomatous hypertrophy of the interatrial septum (n = 1), Marfan's syndrome (n = 1), sinus venosus defect (n = 1), transposition of the great arteries (n = 1), and ventricular arrhythmia (n = 1). Three of the examinations were performed with general anesthesia.

Fig. 3 shows representative 3D cine SSFP images, 3D cine PC GRE (i.e., 4D flow) images and their fusion. Supplementary Video 1 depicts the fusion of 3D cine SSFP images and 3D cine PC flow data in an LV 3-chamber view from the same patient. Supplementary Video 2 shows the fused 3D cine SSFP and PC GRE image set and how it can be reformatted and simultaneously show anatomical and blood flow information.

3.2. Spatial registration

The 3D cine SSFP images were spatially registered to the magnitude images of the 3D cine PC GRE flow images as described above. Table 1 shows the registration parameters between the two datasets. The largest mean inter-scan translation was along the superior-inferior direction and the largest mean inter-scan rotation was along the right-left axis. Registration led to a significantly higher mean Dice coefficient (indicating more overlap) for regions of interest in the transverse aortic arch (pre-registration 83.0 ± 9.6 vs. post-registration 87.8 ± 6.0; P-value < 0.001) and ascending aorta (pre-registration 90.1 ± 4.8 vs. post-registration 91.8 ± 4.2; P-value < 0.001) (Supplementary Figs. 1 and 2). To assess whether the registration process altered the flow data, net ascending aorta blood flow measured using only the 3D cine PC GRE dataset was compared to that measured from the fused (registered) image dataset. There was no statistically significant difference between the measurements (n = 20, 3D cine PC GRE only 61.9 ± 23.2 L/min

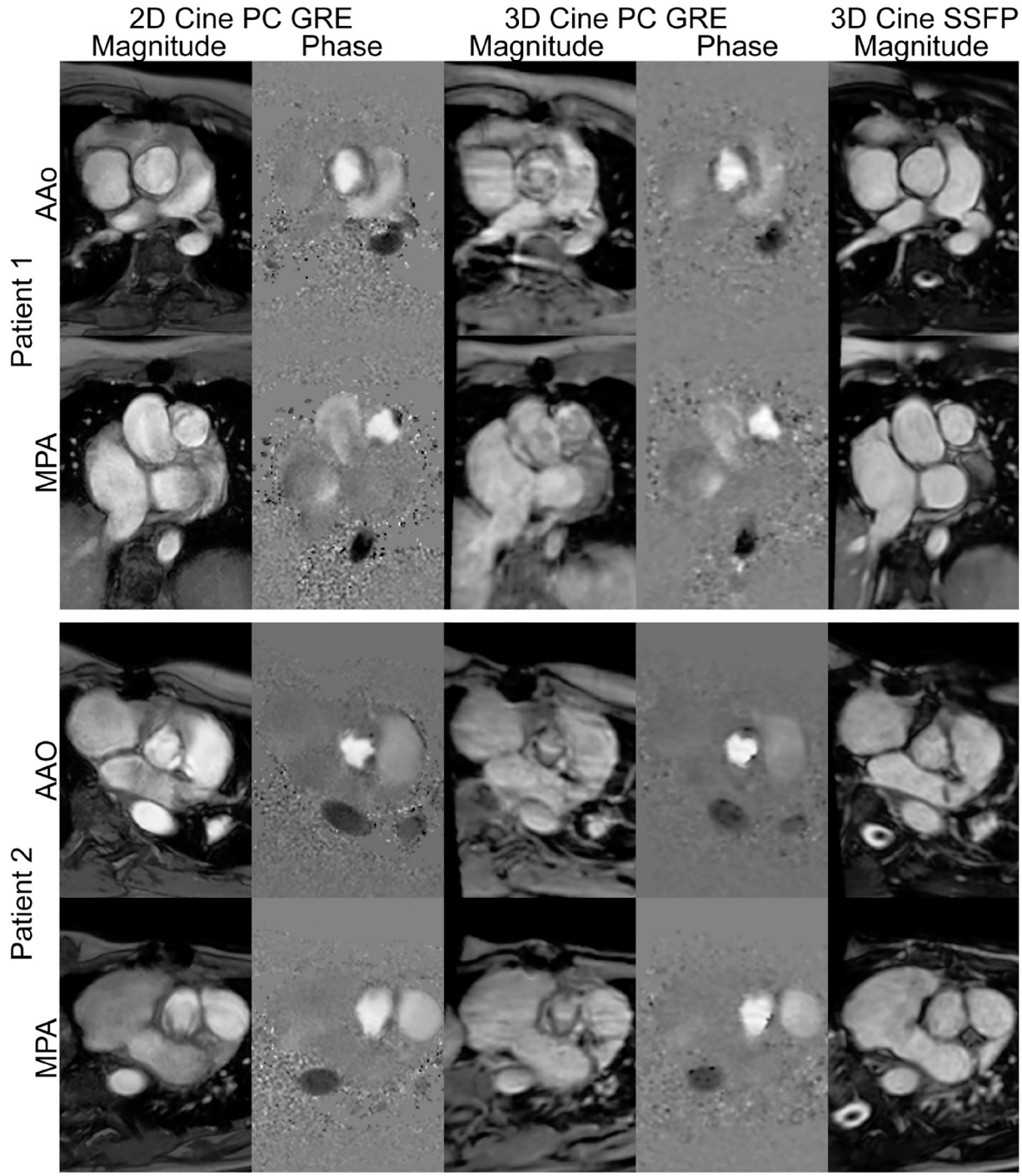

Fig. 6. Comparison of 2D cine PC and 3D cine PC GRE datasets with the fused 3D cine SSFP images though the ascending aorta (AAo) and main pulmonary artery (MPA) from a 19-year-old female patient with repaired tetralogy of Fallot and a 16-year-old female patient with Marfan syndrome.

vs. fused 3D cine PC GRE and 3D cine SSFP 61.2 ± 21.7 L/min; P-value = 0.52).

3.3. Scan time

The scan time of the 3D cine SSFP acquisition was 7.1 ± 1.1 min and of the 3D cine PC GRE acquisition 13.6 ± 3.5 min, resulting in a combined scan time of 20.7 ± 3.8 min. As noted above, the planning time for both of these sequences is short since the imaging plane is not angulated (straight sagittal). The combined planning and scan time for all the 2D cine SSFP (up to 11 different orientations) and 2D cine flow (up to 4 locations) acquisitions was 35.6 ± 8.6 min. This time was significantly longer than the combined 3D cine scan time (P-value < 0.001).

3.4. Ventricular measurements

Mid-ventricular short-axis slices using 2D cine SSFP and 3D cine SSFP are shown in Fig. 4 and Supplementary Video 3. Table 2 and Fig. 5 compare LV and RV measurements between the 2D cine and 3D cine SSFP acquisitions. Of note, for both ventricles EDV was smaller by 3D and ESV was not significantly different. The mean percent difference

Table 3
Blood flow measurements for the 2D cine PC GRE versus fused 3D cine SSFP and PC GRE sequences.

	AAo (L/min)	MPA (L/min)
N	20	17
2D cine PC GRE (flow)	4.7 ± 1.4	5.6 ± 1.2
3D cine SSFP & PC GRE	4.6 ± 1.4	5.1 ± 1.1
Mean difference (3D-2D)	−0.1 ± 0.4	−0.6 ± 0.8
Mean % difference (3D-2D)	−2.6 ± 8.9	−11.2 ± 15.3
Correlation coefficient	0.956	0.738
P-value	0.312	0.010

Values are mean ± standard deviation. AAo, ascending aorta; LPA, left pulmonary artery; MPA, main pulmonary artery; and RPA, right pulmonary artery.

was ≤5% for all parameters.

3.5. Blood flow measurements

Fig. 6 shows representative 2D flow and fused, reformatted 3D cine (i.e., 4D flow) images through the AAo and MPA. Table 3 and Fig. 7 show the comparison between conventional 2D flow versus fused 3D cine net blood flow measurements in the AAo and MPA. Agreement for AAo flow was acceptable (bias −2.6 ± 8.9%) while MPA flow was lower with the fused 3D cine sequence (bias −11.2 ± 15.3%, P = 0.010). The pulmonary-to-systemic blood flow ratio measured from fused 3D cine images (0.95 ± 0.12) was not significantly different than that from the 2D images (1.03 ± 0.08) (P-value = 0.14).

Two comparisons were performed to assess the internal consistency of the fused 3D cine flow data. The mean difference between MPA and the sum of LPA and RPA flow was −0.12 ± 0.55 L/min (mean percent difference − 1.64 ± 9.17%, Cronbach's alpha 0.94). The mean difference between AAo and the sum of SVC and DAo flow was 0.03 ± 0.19 L/min (mean percent difference 0.44 ± 4.11%, Cronbach's alpha 0.99).

4. Discussion

We developed and evaluated in patients a free-breathing and easy to plan 3D cine function and flow CMR examination. This consisted of a nearly isotropic 3D cine SSFP sequence and a nearly isotropic 3D cine PC (i.e., 4D flow) sequence, both with retrospective electrocardiogram gating and prospective respiratory motion compensation. The two image datasets were spatially registered and the SSFP images were substituted for the magnitude images in the PC flow sequence to yield a single 3D cine dataset suitable for a comprehensive analysis of thoracic anatomy, ventricular function, and blood flow. This novel fused dataset facilitates simultaneous visualization of anatomy and blood flow, and easier segmentation compared to a standard 3D cine PC GRE sequence. In a prospective evaluation in patients, all 3D cine SSFP and 3D PC flow acquisitions were completed successfully and the mean scan time including sequence prescription was shorter than that for the corresponding 2D sequences. Compared to the 2D cine acquisition, EDV was smaller by 3D and ESV was not significantly different. Compared to the 2D flow sequence, the fused 3D cine AAo net blood flow was similar and MPA net flow was lower. The pulmonary-to-systemic blood flow ratio measured from the fused 3D cine images was not significantly different than that from the 2D images. The internal consistency of fused 3D cine flow data was good as AAo flow and the sum of SVC and DAo flow were close as was MPA flow and the sum of RPA and LPA flow. Overall, these results show that our fused 3D cine technique may be able to shorten scan time and simplify examination planning.

Left and right ventricular EDV were smaller by 3D cine SSFP than 2D cine SSFP. The biases were all ≤5%, which, for perspective, is in the range reported for inter-scan variability in congenital heart disease patients [27]. The temporal resolution of the 3D and 2D cine datasets was the same. However, the 3D cine data was reformatted into ventricular short-axis slices with a thickness of 5 mm and no gap while the 2D cine images were acquired with a slice thickness of 8 mm and a gap of 0–2 mm. The 3D data had lower in-plane spatial resolution and were acquired after a contrast agent was administered. These differences could have contributed to the lower ventricular volume measurements. In addition, although the 2D and 3D image datasets were both acquired at end-expiration, it is possible that the different breathing patterns (i.e., breath-holding versus free-breathing) contributed to the small discrepancy [28]. The systematic biases we found should be considered when comparing measurements from 3D imaging to a patient's prior 2D imaging data or normal ranges derived from 2D imaging.

The agreement between the fused 3D and 2D net flow measurements was better for the AAo than the MPA. The differences between the 3D and 2D acquisitions regarding through plane resolution and post-contrast imaging may contribute to the overall flow measurement discrepancy; however, it is doubtful that these factors can account for the larger systematic bias for MPA flow. A possible explanation for this result stems from noting that the fused 3D flow sequence was gated to end-expiration while the 2D flow sequence acquired data throughout the respiratory cycle. The systematically lower 3D MPA flow may be because respiratory variation in flow is more pronounced in the pulmonary circulation than in the systemic circulation and pulmonary flow decreases in expiration. In addition, since the MPA is farther from the scanner isocenter than the AAo and has a more oblique orientation, it is more subject to phase offset errors and it is possible the errors were different between the 2D and 3D sequences [29]. Further research into phase offset correction techniques may help resolve this issue.

Compared to the standard 2D cine and 2D PC flow, our fused 3D approach requires several additional post-processing steps. The 3D cine SSFP and 3D cine PC GRE series need to be loaded into the MASS research software and spatially registered. Together, these steps take about 2 min. After the registration, the fused 3D images must be

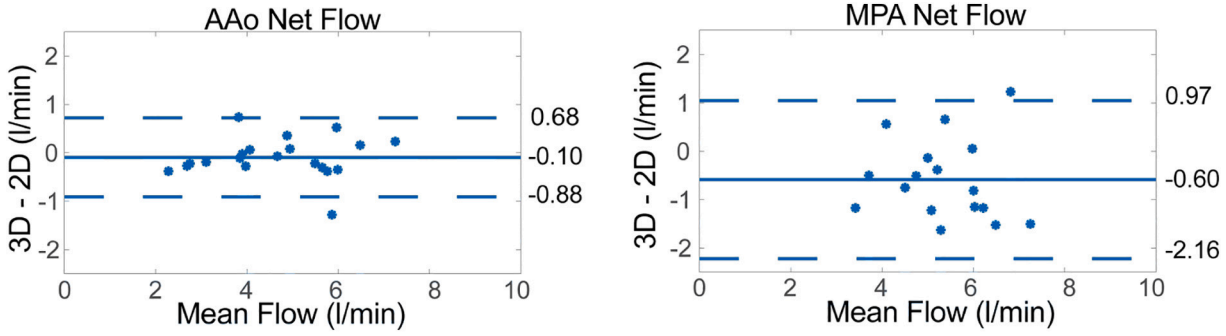

Fig. 7. Bland-Altman plots of agreement comparing systemic and pulmonary blood flow measurements for the conventional 2D cine PC GRE images and free-breathing 3D cine SSFP and 3D PC GRE datasets. The solid line indicates the mean difference (bias) and the dashed lines show ± 1.96 standard deviations of difference.

reformatted into multiple images series for analysis. These reformats include a stack of ventricular short-axis images and a cross-sectional view of the blood vessel at each location where flow is to be measured. Each of these reformats takes less that one minute to create. Future work will explore automatic reformatting and ventricular border detection in 3D space using artificial intelligence.

There has been one other study that aimed to produce a comprehensive 3D cine CMR examination. Hanneman et al. used the iron-based contrast agent, ferumoxytol, to boost the signal from blood and improve the blood-to-myocardium contrast-to-noise ratio of an accelerated 3D cine PC GRE (i.e., 4D flow) sequence [15]. As a result, the magnitude images had sufficient quality to assess anatomy and segment the ventricles. Ferumoxytol, though, has been associated with a significant risk of anaphylactic reactions [17–19] and this has led to restrictions on use and availability in some countries. Our technique, however, employs a gadolinium-based contrast agent to increase the signal from blood and improve the quality of the 3D cine SSFP images. The enhanced 3D cine SSFP images are then used to replace the magnitude images from a second 3D cine sequence, the PC acquisition, which have relatively low contrast even after administering a gadolinium-based contrast agent. Gadolinium-based contrast agents have a lower risk of anaphylactic reactions and are more commonly used in clinical practice; however, they still are associated with some safety concerns [30] and their use necessitates intravenous line placement. In order to avoid the use of any contrast agent with our technique, the 3D cine SSFP images must have a sufficient blood-to-myocardium contrast-to-noise ratio for reliable ventricular segmentation. To this end, Feng et al. periodically interrupted the acquisition to suppress the signal from fat and then drove the net magnetization vector back to the steady-state using 10 startup pulses [8]. Although these periodic interruptions improve the contrast-to-noise ratio of the 3D cine images, they preclude the acquisition of cine data throughout the entire cardiac cycle.

Our study has several limitations. The number of subjects was relatively small and it is thus possible that additional differences between the 3D cine and the conventional 2D cine techniques might emerge with a larger sample size. We had only a few patients who underwent their CMR examinations while sedated. Nevertheless, we would expect that our comprehensive 3D cine examination would perform even more effectively with sedation since patients will usually have a more regular breathing pattern and heart rate. We have not yet systemically optimized the spatial resolution of the 3D cine CMR parameters. In the current study, a $\approx$ 2 mm^3 spatial resolution was chosen because it provided an acceptable balance between image quality, available memory on the scanner and scan time in preliminary trials.

In the future, we plan to explore several enhancements to our comprehensive 3D cine examination technique. Dividing the 3D cine SSFP sequence into multiple slabs or pausing data acquisition to allow recovery of the net magnetization vector may increase the blood signal enough to eliminate the need for intravenous contrast. Application of compressed sensing in space and time to both the 3D cine SSFP and PC flow sequences using a moderate acceleration factor of 6 should reduce the combined scan time to about 10 min. Furthermore, modifying the 3D cine PC sequence to include a second encoding velocity may improve the precision of blood flow measurements. Finally, because our technique does not require special modifications to the scanner for image acquisition and reconstruction, it is readily shared with other sites that have the same scanner manufacturer. A multicenter study is currently underway to evaluate the generalizability of our study findings and to further explore clinical utility.

In conclusion, we developed and evaluated in patients a free-breathing 3D cine CMR examination approach to assess anatomy, ventricular function, and blood flow. Our initial comparisons to the standard 2D cine technique are encouraging. With further refinement and testing, our 3D cine approach has the potential for a CMR examination that is easier to plan, faster and free-breathing; and enables volume-based reformatting with intuitive flow data overlay.

Supplementary data to this article can be found online at https://doi.org/10.1016/j.mri.2020.09.026.

Authors' contributions

All authors contributed significantly to this manuscript. All authors read, reviewed, and approved the final manuscript. Mehdi H. Moghari: study design, method development, MRI scanning, data analysis, manuscript writing, and funding acquisition; Rob J. van der Geest, Maurizio Brighenti, and Andrew J. Powell: data analysis and manuscript writing.

Funding sources

Dr. Moghari was supported by the Office for Faculty Development at Boston Children's Hospital, Charles H. Hood Foundation and NIH R01 grant (R01 HL149807–01).

Declaration of Competing Interest

None.

References

[1] Kramer CM, Barkhausen J, Flamm SD, Kim RJ, Nagel E. Standardized cardiovascular magnetic resonance (CMR) protocols 2013 update. J Cardiovasc Magn Reson 2013;15(1):91.
[2] Jahnke C, Paetsch I, Achenbach S, Schnackenburg B, Gebker R, Fleck E, et al. Coronary MR imaging: breath-hold capability and patterns, coronary artery rest periods, and beta-blocker use. Radiology 2006;239(1):71–8.
[3] Swingen C, Seethamraju RT, Jerosch-Herold M. An approach to the three-dimensional display of left ventricular function and viability using MRI. Int J Cardiovasc Imaging 2003;19(4):325–36.
[4] Uribe S, Muthurangu V, Boubertakh R, Schaeffter T, Razavi R, Hill DL, et al. Whole-heart cine MRI using real-time respiratory self-gating. Magn Reson Med 2007;57(3):606–13.
[5] Pang J, Sharif B, Fan Z, Bi X, Arsanjani R, Berman DS, et al. ECG and navigator-free four-dimensional whole-heart coronary MRA for simultaneous visualization of cardiac anatomy and function. Magn Reson Med 2014;72(5):1208–17.
[6] Coppo S, Piccini D, Bonanno G, Chaptinel J, Vincenti G, Feliciano H, et al. Free-running 4D whole-heart self-navigated golden angle MRI: initial results. Magn Reson Med 2015;74(5):1306–16.
[7] Han F, Rapacchi S, Khan S, Ayad I, Salusky I, Gabriel S, et al. Four-dimensional, multiphase, steady-state imaging with contrast enhancement (MUSIC) in the heart: a feasibility study in children. Magn Reson Med 2015;74(4):1042–9.
[8] Feng L, Coppo S, Piccini D, Yerly J, Lim RP, Masci PG, et al. 5D whole-heart sparse MRI. Magn Reson Med 2017. https://doi.org/10.1002/mrm.26745.
[9] Usman M, Ruijsink B, Nazir MS, Cruz G, Prieto C. Free breathing whole-heart 3D CINE MRI with self-gated Cartesian trajectory. Magn Reson Imaging 2017;38:129–37.
[10] Miller S, Simonetti OP, Carr J, Kramer U, Finn JP. MR imaging of the heart with cine true fast imaging with steady-state precession: influence of spatial and temporal resolutions on left ventricular functional parameters. Radiology 2002;223(1):263–9.
[11] Inoue Y, Nomura Y, Nakaoka T, Watanabe M, Kiryu S, Okubo T, et al. Effect of temporal resolution on the estimation of left ventricular function by cardiac MR imaging. Magn Reson Imaging 2005;23(5):641–5.
[12] Uribe S, Beerbaum P, Sorensen TS, Rasmusson A, Razavi R, Schaeffter T. Four-dimensional (4D) flow of the whole heart and great vessels using real-time respiratory self-gating. Magn Reson Med 2009;62(4):984–92.
[13] Lai LM, Cheng JY, Alley MT, Zhang T, Lustig M, Vasanawala SS. Feasibility of ferumoxytol-enhanced neonatal and young infant cardiac MRI without general anesthesia. J Magn Reson Imaging 2017;45(5):1407–18.
[14] Cheng JY, Hanneman K, Zhang T, Alley MT, Lai P, Tamir JI, et al. Comprehensive motion-compensated highly accelerated 4D flow MRI with ferumoxytol enhancement for pediatric congenital heart disease. J Magn Reson Imaging 2016;43(6):1355–68.
[15] Hanneman K, Kino A, Cheng JY, Alley MT, Vasanawala SS. Assessment of the precision and reproducibility of ventricular volume, function, and mass measurements with ferumoxytol-enhanced 4D flow MRI. J Magn Reson Imaging 2016;44(2):383–92.
[16] Han F, Zhou Z, Han E, Gao Y, Nguyen KL, Finn JP, et al. Self-gated 4D multiphase, steady-state imaging with contrast enhancement (MUSIC) using rotating cartesian K-space (ROCK): validation in children with congenital heart disease. Magn Reson Med 2017;78(2):472–83.
[17] Rubin R. Black box warning for anemia drug. JAMA 2015;313(17):1704.
[18] DeLoughery TG. Risk of anaphylaxis with intravenous iron products. JAMA 2016;315(20):2232.

[19] U.S. Food and Drug Administration: Feraheme (ferumoxytol): Drug Safety Communication – Warnings Strengthened and Prescribing Instructions Changed. 2015.
[20] Moghari MH, Geva T, Powell AJ. Prospective heart tracking for whole-heart magnetic resonance angiography. Magn Reson Med 2017;77(2):759–65.
[21] Moghari MH, Barthur A, Amaral ME, Geva T, Powell AJ. Free-breathing whole-heart 3D cine magnetic resonance imaging with prospective respiratory motion compensation. Magn Reson Med 2018;80(1):181–9.
[22] Moghari MH, Chan RH, Hong SN, Shaw JL, Goepfert LA, Kissinger KV, et al. Free-breathing cardiac MR with a fixed navigator efficiency using adaptive gating window size. Magn Reson Med 2012;68(6):1866–75.
[23] Klein S, Staring M, Murphy K, Viergever MA, Pluim JP. Elastix: a toolbox for intensity-based medical image registration. IEEE Trans Med Imaging 2010;29(1):196–205.
[24] Buehrer M, Pruessmann KP, Boesiger P, Kozerke S. Array compression for MRI with large coil arrays. Magn Reson Med 2007;57(6):1131–9.
[25] Bland JM, Altman DG. Statistical methods for assessing agreement between two methods of clinical measurement. Lancet 1986;1(8476):307–10.
[26] Cronbach LJ. Coefficient alpha and the internal structure of tests. Psychometrika 1951;16(3):297–334.
[27] Blalock SE, Banka P, Geva T, Powell AJ, Zhou J, Prakash A. Interstudy variability in cardiac magnetic resonance imaging measurements of ventricular volume, mass, and ejection fraction in repaired tetralogy of Fallot: a prospective observational study. J Magn Reson Imaging 2013;38(4):829–35.
[28] Reyhan ML, Wang Z, Kim HJ, Halnon NJ, Finn JP, Ennis DB. Effect of free-breathing on left ventricular rotational mechanics in healthy subjects and patients with duchenne muscular dystrophy. Magn Reson Med 2017;77(2):864–9.
[29] Hanneman K, Sivagnanam M, Nguyen ET, Wald R, Greiser A, Crean AM, et al. Magnetic resonance assessment of pulmonary (QP) to systemic (QS) flows using 4D phase-contrast imaging: pilot study comparison with standard through-plane 2D phase-contrast imaging. Acad Radiol 2014;21(8):1002–8.
[30] Ranga A, Agarwal Y, Garg KJ. Gadolinium based contrast agents in current practice: risks of accumulation and toxicity in patients with normal renal function. Indian J Radiol Imag 2017;27(2):141–7.